VIP Heterogeneous Catalysis

DOI: 10.1002/anie.200904282

Label-Free Chemical Imaging of Catalytic Solids by Coherent Anti-Stokes Raman Scattering and Synchrotron-Based Infrared Microscopy**

*Marianne H. F. Kox, Katrin F. Domke, James P. R. Day, Gianluca Rago, Eli Stavitski, Mischa Bonn, and Bert M. Weckhuysen**

Worldwide environmental restrictions on sulfur levels in gasoline have prompted the need for increasingly selective sulfur-removing catalysts. Zeolites have proven to be effective additives for the removal of sulfur-containing species during catalytic cracking processes. Whereas the structural building blocks of individual zeolite crystals are well understood and detailed reaction pathways on the molecular level have been proposed, the link between the macroscopic and molecular worlds, namely, the correlation of the crystal's internal architecture and catalytic activity on the micrometer scale, has remained elusive. It is often assumed that a catalytic reaction occurs homogeneously throughout a zeolite crystal, not taking into consideration the role of the porous network, grain boundaries, or defect sites on the distribution of reactants and formation of reaction intermediates and products. A microscopic picture of what happens throughout an individual zeolite crystal is lacking. Three-dimensional, high-resolution chemical maps of the spatial distribution of catalytic species within crystal zeolites would provide unprecedented insight into the structure–reactivity relationship, which could lead to the design of improved catalysts.[1,2]

Herein, we propose a unique combination of multiplex coherent anti-Stokes Raman scattering (CARS) and synchrotron-based infrared (IR) microspectroscopy experiments to achieve this goal. The latter, employing a light source 100–1000 times brighter than conventional IR light, has been shown to be a powerful tool for obtaining two-dimensional (2D) chemical maps with micrometer spatial resolution of a solid acid in the course of a catalytic reaction.[3,4] These efforts are complemented here with CARS microscopy, thus allowing z sectioning (3D imaging) at even better spatial resolution. CARS is several orders of magnitude more sensitive than normal Raman spectroscopy and possesses an intrinsic sectioning capability of approximately 400 nm in the x and y directions and approximately 1 μm in the z direction, thus enabling 3D chemical mapping of small amounts of analytes in confined space with micrometer or sub-micrometer resolution.[5–9] In contrast to the more routinely employed (confocal) fluorescence microscopy,[10–15] CARS and IR vibrational signatures provide intrinsic chemical information about the species of interest and their interaction with the environment, without the need for fluorescent or fluorescently labeled species. Details on the experimental setups can be found in the Supporting Information.

We report the catalytic conversion of thiophene derivatives within individual H-ZSM-5 crystals in microscopic detail. We present multidimensional, label-free chemical maps of micrometer resolution of reactant as well as reaction intermediates and products that reveal an inhomogeneous distribution of active species throughout the zeolite crystals. The spectral changes that occur upon adsorption of the thiophene derivatives allow us to monitor in situ the interaction of the reactants with the zeolite and the consecutive cation formation and ring-opening reactions.

To visualize the distribution of thiophene reactants prior to catalytic conversion, coffin-shaped H-ZSM-5 crystals ($100 \times 20 \times 20\ \mu m^3$) were exposed to differently substituted thiophene derivatives and left at room temperature for approximately 30 min to ensure all excess thiophene had evaporated. Subsequently, space-resolved CARS spectra were recorded on individual H-ZSM-5 crystals, which were analyzed using the maximum entropy method (MEM).[16] This method provides the quantitative Raman response, which will be referred to as "nonlinear Raman response". Below, 2-chlorothiophene is used as an example. Results obtained for other thiophene derivatives and details on the MEM analysis procedure can be found in the Supporting Information. In Figure 1a, the nonlinear Raman response of 2-chlorothiophene and an H-ZSM-5 crystal containing 2-chlorothiophene are presented for the C–H stretching region (3250–2950 cm^{-1}). Examination of the response for the zeolite containing 2-chlorothiophene shows the presence of a band at 3078 cm^{-1} and a pronounced band at 3115 cm^{-1} with a

[*] M. H. F. Kox, Dr. E. Stavitski, Prof. Dr. B. M. Weckhuysen
Inorganic Chemistry and Catalysis Group
Debye Institute for Nanomaterials Science, Utrecht University
Sorbonnelaan 16, 3584 CA, Utrecht (The Netherlands)
Fax: (+31) 30-251-1027
E-mail: b.m.weckhuysen@uu.nl
Dr. K. F. Domke, Dr. J. P. R. Day, G. Rago, Prof. Dr. M. Bonn
Biosurface Spectroscopy
FOM Institute for Atomic and Molecular Physics
Science Park 113, 1098 XG Amsterdam (The Netherlands)

[**] We thank the Dutch National Science Foundation (NWO CW VICI, VENI and TOP Grant) and Research School Combination Catalysis (NRSC-C) for financial support. Dr. M. Mertens (ExxonMobil) is acknowledged for providing the H-ZSM-5 crystals; Dr. T. Visser, R. Smith (NSLS), and Dr. L. Miller (NSLS) are thanked for assistance with the IR spectroscopy measurements. The National Synchrotron Light Source (NSLS) is supported by the U.S. Department of Energy, Office of Science, Office of Basic Energy Sciences under contract DE-AC02-98CH10886. K.F.D. thanks the Alexander von Humboldt Foundation (Germany) for a Feodor Lynen fellowship.

Supporting information for this article is available on the WWW under http://dx.doi.org/10.1002/anie.200904282.

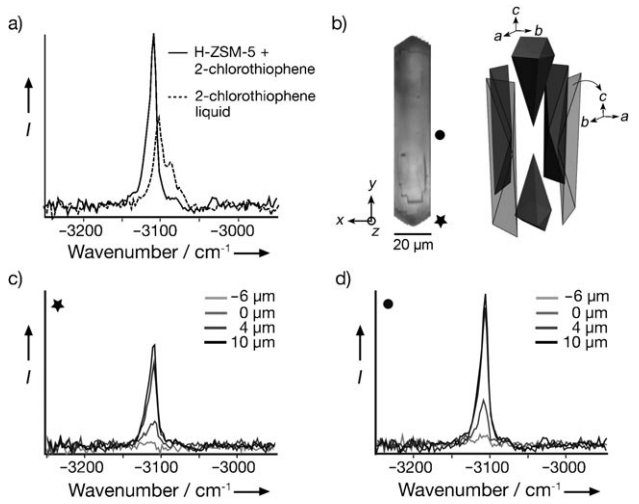

Figure 1. a) Nonlinear Raman responses for 2-chlorothiophene and an H-ZSM-5 crystal containing 2-chlorothiophene, displayed for the C–H stretching region. b) Microphotograph of an individual H-ZSM-5 crystal along with a schematic representation of the crystal's intergrowth structure and crystallographic orientations (*a*,*b*,*c*). The (*x*,*y*,*z*) vectors indicate the overall dimensions. c) Nonlinear Raman responses measured at the edge of the crystal for different *z* positions. d) Same as (c) but for the crystal's center.

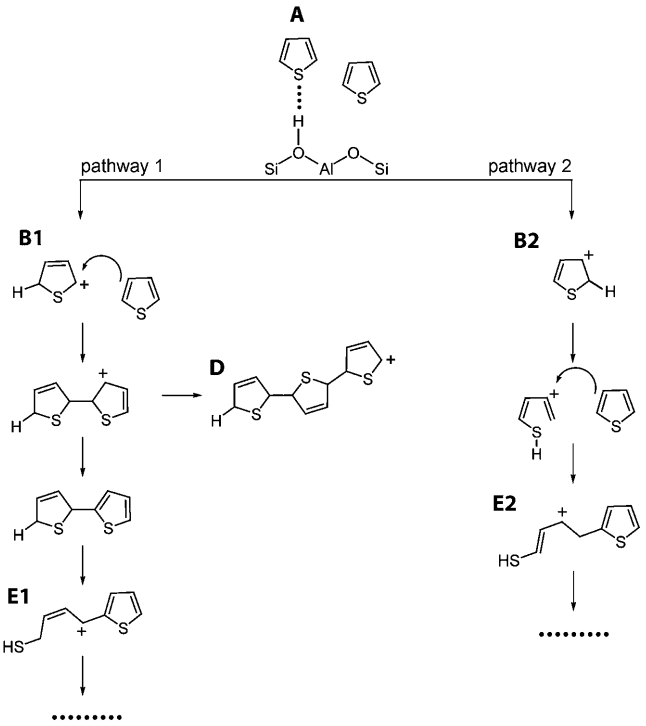

Scheme 1. Possible reaction pathways of thiophene on acidic zeolites. See text for details.

bandwidth of approximately 13 cm^{-1} (full width at half maximum), assigned to =C–H stretching vibrations of an intact thiophene ring. The nonlinear Raman response of the bulk liquid reveals prominent bands at 3105, 3091, and 3075 cm^{-1}. Assuming similar pathways for the reaction of 2-chlorothiophene with H-ZSM-5 zeolites, we refer to reaction pathways proposed in the literature for the conversion of unsubstituted thiophenes (Scheme 1).[17–23] The initial reaction step is the hydrogen bonding of a thiophene monomer to the zeolite framework (**A**) with subsequent formation of an initial thiophene carbocation (**B1**,**B2**). In pathway 1, oligomerization of the carbocation with a thiophene monomer leads to the formation of a thiophene dimer, which can either further oligomerize (structure **D**) or (partially) crack, involving opening of the thiophene ring (structure **E1**). In pathway 2, after formation of carbocation **B2**, direct opening of the thiophene ring occurs. Subsequent reaction with another thiophene monomer leads to the formation of molecule **E2**. Depending on the reaction conditions, further reactions (e.g., cracking) can take place after the formation of molecules **E1** and **E2**. Note that in the case of 2-chlorothiophene, owing to the substitution of the C2-position and concurrent steric hindrance effects, formation of molecule **D** would not be feasible. Consecutive reaction steps under various reaction conditions have been discussed and calculated in detail in the literature.[24–26] The observed spectral changes in the nonlinear Raman spectra upon the inclusion of 2-chlorothiophene in the zeolite provide clear evidence for the interaction of the reactant with the catalyst framework, for example, by means of hydrogen bonding (Scheme 1, structure **A**), which is known to occur at room temperature.[20]

In Figure 1 b, a microphotograph of an individual H-ZSM-5 crystal is presented, along with a schematic representation illustrating the crystal's intergrowth structure and crystallographic orientations.[27,28] Within the H-ZSM-5 crystals, which have a two-dimensional pore network with interconnected straight and sinusoidal pores, the direction of the straight pores is parallel to the crystallographic *b* axis. The nonlinear Raman responses of 2-chlorothiophene as a function of depth within the crystal are presented in Figure 1 c,d for the edge (★) and center (●) regions, respectively. Quantitative evaluation of these spectra reveals that approximately twice as much reactant is present in the center of the crystal than near the edges. This observation has two likely causes: 1) Capillary forces induced by the zeolite's micropores, which are enhanced by the presence of a 90° rotational intergrowth structure, separating the edge from the center subunit. Owing to the mismatch in pore alignment between these regions, migration of 2-chlorothiophene monomers from one subunit to another is severely hindered. As a result, for the pyramidal edge subunit stretching out to the crystal's center, 2-chlorothiophene reactants are directed towards the middle of the crystal by the imposed capillary forces. 2) The effect of laser heating facilitates evaporation of reactants from the outer surface regions.

In a second set of experiments, an individual H-ZSM-5 crystal was raster scanned in three dimensions, with steps of 1 μm in the *x* and *y* directions and 2 μm in the *z* direction. 2D nonlinear Raman response images for the lower edge region are presented in Figure 2. The intensity of the 3115 cm^{-1} band is plotted for different *x*,*y*,*z* positions. These plots show striking similarity with the microphotograph presented in Figure 1 b. The very high resolution of the CARS images visualizes small intensity changes on the micrometer scale and

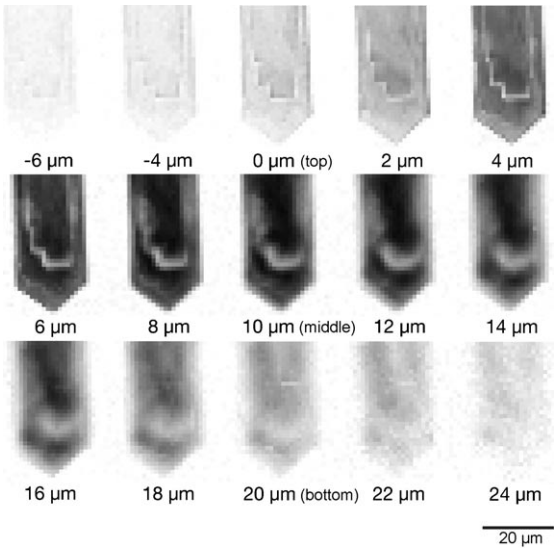

Figure 2. 2D nonlinear Raman response images of the normalized band at 3115 cm^{-1} as a function of position. The top of the crystal is set to 0 µm, −4 µm equals 4 µm outside (above) the crystal. The images are color-coded in grayscale; that is, the darker the pixel, the more 2-chlorothiophene reactant present.

the increase of reactant concentration towards the middle of the crystal as well as along defects. Similar results were observed at the upper edge region of the crystal (see the Supporting Information). Subsequently, 3D images were reconstructed. The result is displayed in Figure 3 a–c for the lower edge and in Figure 3 d–f for the upper edge of the H-ZSM-5 crystal. Approximately 2.5 times more reactant is present in the middle than in the outer crystal regions. This inhomogeneous reactant distribution is clearly visible in Figure 3 f, where an hourglass pattern can be observed, illustrating the effect of intergrowth barriers on reactant diffusion. It is important to ensure that the influence of refraction is negligible.[29] For this purpose, a blank H-ZSM-5 crystal was mapped. The result is presented in Figure 3 g–i, in which the intensity of the 2320 cm^{-1} band is plotted (assigned to the gas-phase stretching vibration of N_2 confined within the zeolite). The nonlinear Raman response spectra and corresponding 2D plots can be found in the Supporting Information. Taking the stepsize of 2 µm for the z direction into consideration, it can be deduced that the boundaries of the 3D crystal images are in excellent agreement with the real crystal dimensions, that is, 20 µm in x and y, respectively.

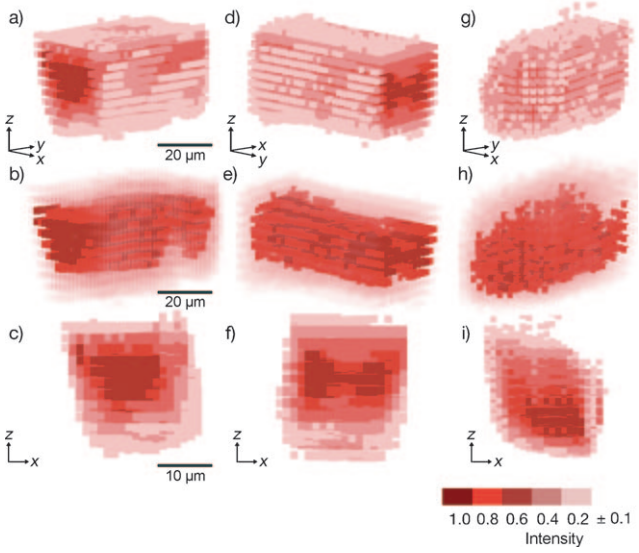

Figure 3. 3D nonlinear Raman response images. a–c) 2-chlorothiophene concentration, based on 3115 cm^{-1} band intensity for the lower edge. d–f) Same as (a–c) but for the upper edge of the crystal in Figure 1 b. Note: (a) and (d) are identical to (b) and (e), but illustrated in opaque. g–i) The same as (a–c) but for the 2320 cm^{-1} band of gas-phase N_2 in a blank H-ZSM-5 crystal. Scale bar indicates the normalized intensity. The tolerance was set to 0.1.

Unfortunately, attempts to map the distribution of reaction products during the catalytic conversion using CARS have not been very successful to date, owing to the formation of fluorescent species resulting in two-photon fluorescence. We therefore reverted to IR microscopy to map product distributions inside the zeolite crystals.

In Figure 4 a, IR reference spectra of 2-chlorothiophene and a blank zeolite H-ZSM-5 crystal are displayed. The presence of zeolite framework bands limits the spectral window of the IR measurements to the ring vibration (1600–1300 cm^{-1}) and C–H stretching region (3300–2700 cm^{-1}). Upon exposure of the H-ZSM-5 crystals to thiophene derivatives and heat treatment at 493 K, the crystals became intensely colored owing to the formation of light-absorbing species, for example, carbocations (Scheme 1). This change is visualized in Figure 4 b, which presents a microphotograph of a crystal after reaction, showing distinct coloration between the edge and the center. Figure 4 c, d displays IR absorption spectra of the 1600–1300 cm^{-1} region recorded in the crystal center for different reaction times and incident polarization directions ($\| y$ and $\perp y$). Comparison with the 2-chlorothiophene reference shows that the bands located at 1346 (C–H bending), 1412, and 1520 cm^{-1} (fundamental ring stretching) are vibrations attributed to the 2-chlorothiophene monomer.[30,31] The observation that these bands are not very dependent on the polarization angle (see Figure 4 e for the 1412 cm^{-1} band) confirms the assignment to small, flexible, and freely rotating monomers. However, the band intensity is not completely independent of the light polarization, thus giving evidence of the presence of hydrogen-bonded 2-chlorothiophene in a first reaction step. Examination of the IR spectra with polarization $\| y$ shows the appearance of three pronounced bands located at 1401, 1506, and 1550 cm^{-1} as the reaction progresses. These bands can be assigned to ring stretching vibrations of (aromatic) reaction products.[30,31] The presence of the 1401 cm^{-1} band after 5 min of reaction indicates that product molecules are formed in the early stages of reaction. Apart from that, the strong dependence of the product bands on the polarization angle (Figure 4 e for the 1401 cm^{-1} band) shows that they must be due to elongated molecules entrapped and aligned within the micropores of the zeolite. The higher intensity at light polarization $\| y$ implies that the transition moment associated with the vibrational modes is directed parallel to the crystal y axis. On the basis of

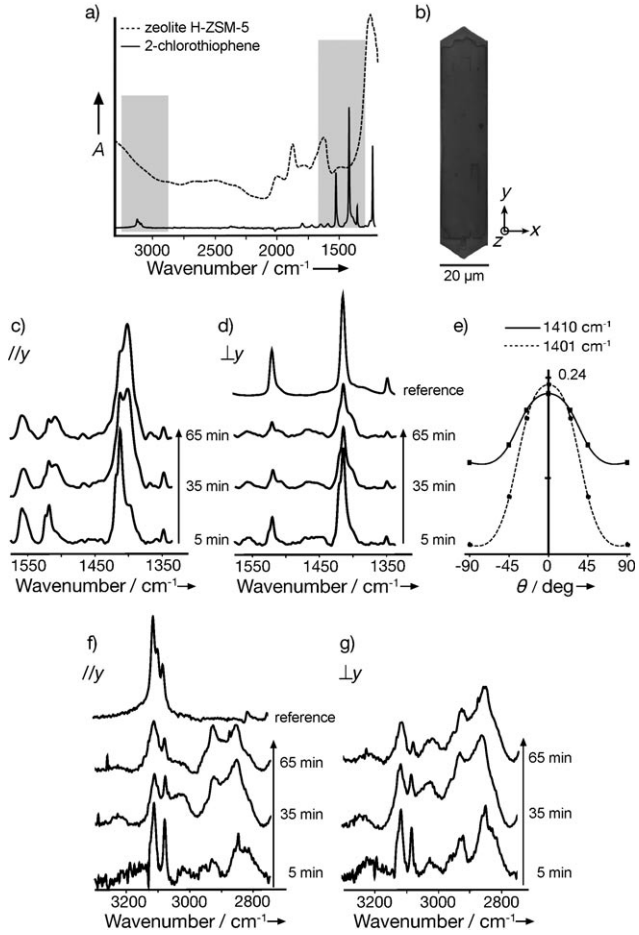

Figure 4. a) IR reference spectra of liquid 2-chlorothiophene and an H-ZSM-5 crystal. b) Microphotograph of a 2-chlorothiophene/H-ZSM-5 crystal after heat treatment at 493 K. c) IR spectra of the ring stretching region measured in the center of the crystal after 5, 35, and 65 min of reaction. The incident polarization was set to $\parallel y$. d) The same as (c) but for light polarization $\perp y$. e) Dependence of the 1412 and 1401 cm^{-1} band intensities on the polarization angle. f, g) The same as (c, d) but for the (enlarged) C–H stretching region. The polarization directions are indicated in (b).

earlier findings on the oligomerization of styrene derivatives along with the presence of a 90° rotational intergrowth structure, it can be rationalized that the product molecules are aligned and accommodated within the straight pores of the zeolite.[4,27,28,32] Moreover, the continuous presence of the ring vibrations of both reactant and products strongly suggests that a considerable part of the thiophene rings remain intact. Finally, it is important to stress that only in the case of the correct polarization direction, in this case $\parallel y$, could bands attributed to vibrations of product molecules be visualized.

More insight into the type of elongated products formed was obtained from investigation of the C–H stretching region (Figure 4 f,g). Firstly, two intense sharp bands at 3110 and 3080 cm^{-1} can be distinguished, which are in perfect agreement with the bands found in the CARS measurements. The former band can be ascribed to the presence of =C–H bonds at multiple positions on the 2-chlorothiophene ring. The latter could originate from both aromatic and olefinic =C–H stretching vibrations[30,31] and therefore might suggest the presence of molecule **E** in Scheme 1. Additionally, two bands located around 2930 and 2850 cm^{-1} are present, which are attributed to aliphatic $-CH_2-$ stretching vibrations.[30,31] These IR bands, along with the coloration of the crystal, are in line with the presence of molecule **E**. Unfortunately, no evidence for the presence of S–H vibrations has been obtained. The corresponding band is intrinsically weak, and interference patterns cover the 2500 cm^{-1} spectral region. More experimental evidence would be possible by examination of the C=C region; however, owing to the limited spectral window, these assignments were not feasible. The complexity of the bands in the 2950–2850 cm^{-1} region could be used as an argument for the presence of an aliphatic C–H stretching band, although no direct evidence can be provided.

In a final series of experiments, the distribution of the 2-chlorothiophene reactant (1412 cm^{-1}) and elongated product (1401 cm^{-1}) over the H-ZSM-5 crystal was mapped. Figure 5 shows spatial maps of the crystal for both reactant and product after 10, 20, and 65 min of reaction. It is important to note that the intensity scale in each 2D map is different. First, it can be seen that as the reaction proceeds the intensity of the reactant band decreases with respect to the band of the reaction product. Furthermore, in the edge region less reactant and product are present, regardless of the reaction time. These observations are in perfect agreement with the results obtained by CARS measurements. Furthermore, taking the intergrowth structure and concurrent diffusion barriers into consideration, it is logical to assume that at locations where less reactant is present, fewer reaction products will be formed.

In summary, the combination of label-free CARS and IR spectral imaging is a powerful tool for studying the multidimensional distribution of thiophene reactants and products in zeolite crystals with micrometer resolution. The accumulation of active species in specific regions of the crystals

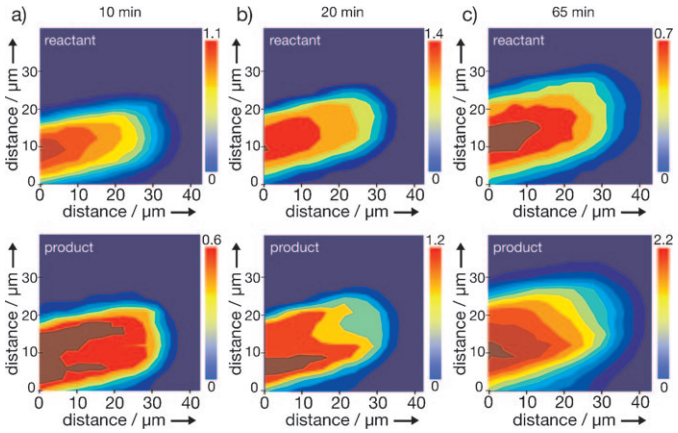

Figure 5. 2D IR intensity maps of a 2-chlorothiophene/H-ZSM-5 crystal after a) 10, b) 20, and c) 65 min of reaction for the 1412 cm^{-1} reactant band (top) and 1401 cm^{-1} product band (bottom). The images are presented as temperature maps. Note: the intensity scale is different for each 2D image. The light polarization was set to $\parallel y$ for all measurements.

illustrates the importance of diffusion barriers and capillary forces imposed by the pore network for the catalytic activity. Spectral changes occurring upon adsorption directly visualize the interaction of the reactants with the zeolite. Strong spectroscopic evidence for the occurrence of hydrogen bonding and opening of the thiophene ring is provided. Importantly, provided by the high spatial resolution of the multiplex CARS methodology, extrapolation of these results to real industrial-sized individual catalyst particles could become viable. This unique correlative approach could become an indispensable tool to advance our understanding of catalytic reactions on the micrometer scale under reaction conditions, thus introducing state-of-the-art chemical imaging techniques to the field of heterogeneous catalysis.

Received: July 31, 2009
Published online: October 12, 2009

Keywords: CARS (coherent anti-Stokes Raman scattering) · heterogeneous catalysis · IR spectroscopy · thiophenes · zeolites

[1] B. M. Weckhuysen, *Angew. Chem.* **2009**, *121*, 5008 – 5043; *Angew. Chem. Int. Ed.* **2009**, *48*, 4910 – 4943.
[2] A. Urakawa, A. Baiker, *Top. Catal.* **2009**, *52*, 1312 – 1322.
[3] L. M. Miller, R. J. Smith, *Vib. Spectrosc.* **2005**, *38*, 237 – 240.
[4] E. Stavitski, M. H. F. Kox, I. Swart, F. M. F. de Groot, B. M. Weckhuysen, *Angew. Chem.* **2008**, *120*, 3599 – 3603; *Angew. Chem. Int. Ed.* **2008**, *47*, 3543 – 3547.
[5] J. X. Cheng, X. S. Xie, *J. Phys. Chem. B* **2004**, *108*, 827 – 840.
[6] C. L. Evans, X. S. Xie, *Annu. Rev. Anal. Chem.* **2008**, *1*, 883 – 909.
[7] W. Min, S. Lu, G. R. Holtom, X. S. Xie, *ChemPhysChem* **2009**, *10*, 344 – 347.
[8] D. Schafer, J. A. Squier, J. van Maarseveen, D. Bonn, M. Bonn, M. Muller, *J. Am. Chem. Soc.* **2008**, *130*, 11592 – 11593.
[9] A. Zumbusch, G. R. Holtom, X. S. Xie, *Phys. Rev. Lett.* **1999**, *82*, 4142 – 4145.
[10] M. B. J. Roeffaers, B. F. Sels, H. Uji-i, F. C. De Schryver, P. A. Jacobs, D. E. De Vos, J. Hofkens, *Nature* **2006**, *439*, 572 – 575.
[11] M. B. J. Roeffaers, J. Hofkens, G. De Cremer, F. C. De Schryver, P. A. Jacobs, D. E. De Vos, B. F. Sels, *Catal. Today* **2007**, *126*, 44 – 53.
[12] E. Stavitski, M. H. F. Kox, B. M. Weckhuysen, *Chem. Eur. J.* **2007**, *13*, 7057 – 7065.
[13] D. Mores, E. Stavitski, M. H. F. Kox, J. Kornatowski, U. Olsbye, B. M. Weckhuysen, *Chem. Eur. J.* **2008**, *14*, 11320 – 11327.
[14] T. Tachikawa, T. Majima, *Langmuir* **2009**, *25*, 7791 – 7802.
[15] W. L. Xu, J. S. Kong, Y. T. E. Yeh, P. Chen, *Nat. Mater.* **2008**, *7*, 992 – 996.
[16] E. M. Vartiainen, H. A. Rinia, M. Muller, M. Bonn, *Opt. Express* **2006**, *14*, 3622 – 3630.
[17] C. L. Garcia, J. A. Lercher, *J. Phys. Chem.* **1992**, *96*, 2669 – 2675.
[18] C. L. Garcia, J. A. Lercher, *J. Mol. Struct.* **1993**, *293*, 235 – 238.
[19] G. Spoto, F. Geobaldo, S. Bordiga, C. Lamberti, D. Scarano, A. Zecchina, *Top. Catal.* **1999**, *8*, 279 – 292.
[20] S. Y. Yu, J. Garcia-Martinez, W. Li, G. D. Meitzner, E. Iglesia, *Phys. Chem. Chem. Phys.* **2002**, *4*, 1241 – 1251.
[21] B. R. Li, W. P. Guo, S. P. Yuan, J. Hu, J. G. Wang, H. J. Hao, *J. Catal.* **2008**, *253*, 212 – 220.
[22] A. Chica, K. Strohmaier, E. Iglesia, *Langmuir* **2004**, *20*, 10982 – 10991.
[23] L. Jaimes, M. L. Ferreira, H. de Lasa, *Chem. Eng. Sci.* **2009**, *64*, 2539 – 2561.
[24] X. Rozanska, X. Saintigny, R. A. van Santen, S. Clemendot, F. Hutschka, *J. Catal.* **2002**, *208*, 89 – 99.
[25] X. Rozanska, R. A. van Santen, F. Hutschka, *J. Catal.* **2001**, *200*, 79 – 90.
[26] X. Saintigny, R. A. van Santen, S. Clemendot, F. Hutschka, *J. Catal.* **1999**, *183*, 107 – 118.
[27] E. Stavitski, M. R. Drury, D. A. M. de Winter, M. H. F. Kox, B. M. Weckhuysen, *Angew. Chem.* **2008**, *120*, 5719 – 5722; *Angew. Chem. Int. Ed.* **2008**, *47*, 5637 – 5640.
[28] L. Karwacki, M. H. F. Kox, M. R. Drury, J. D. Meeldijk, E. Stavitski, W. Schmidt, M. Mertens, P. Cubillas, N. John, A. Chan, N. Kahn, S. R. Bare, M. Anderson, J. Kornatowski, B. M. Weckhuysen, *Nat. Mater.* **2009**, DOI: 10.1038/NMAT2530.
[29] N. Djaker, D. Gachet, N. Sandeau, P. F. Lenne, H. Rigneault, *Appl. Opt.* **2006**, *45*, 7005 – 7011.
[30] D. Lin-Vien, N. B. Colthup, W. G. Fateley, J. G. Grasselli, *The Handbook of Infrared and Raman Characteristic Frequencies of Organic Molecules*, Academic Press, New York, **1991**.
[31] G. Socrates, *Infrared Characteristic Group Frequencies*, Vol. 2, Wiley, **1994**.
[32] M. H. F. Kox, E. Stavitski, B. M. Weckhuysen, *Angew. Chem.* **2007**, *119*, 3726 – 3729; *Angew. Chem. Int. Ed.* **2007**, *46*, 3652 – 3655.

